Available online at www.sciencedirect.com

ScienceDirect

Mendeleev Commun., 2021, **31**, 532–535

Mendeleev Communications

Effect of spin polarization and supercell size on specific energy and electronic structure of MoS_2 edge calculated by DFT method in the plane-wave basis

Eugenii A. Permyakov, Vladimir V. Maximov and Victor M. Kogan*

N. D. Zelinsky Institute of Organic Chemistry, Russian Academy of Sciences, 119991 Moscow, Russian Federation. E-mail: vmk@ioc.ac.ru

DOI: 10.1016/j.mencom.2021.07.032

The effect of supercell size in the ribbon model of molybdenum disulfide edge on the cell electronic structure and specific energy was investigated, with and without spin polarization. The differences found were discussed in terms of electron count. Diagnostic criteria for the model applicability and the effect of opposite edge were discussed.

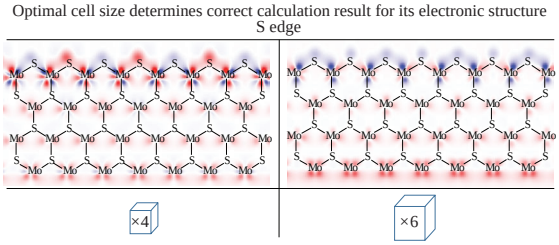

Keywords: DFT, transition metal sulfide catalysts, MoS_2, electronic structure, synthesis gas.

MoS_2 derived systems are crucial catalysts of key processes in modern oil refining.[1] They are used in the alcohol synthesis[2] from syngas and in various hydrogenation processes.[3–5] Numerous computational studies of the active centers of these systems focus on the structure and properties of the edge of molybdenum sulfide.[6–12] Also, various layered dichalcogenides are being studied in solid state physics and materials science as promising semiconductors.[13–15] Many studies are devoted, in particular, to the properties of the edge of a monolayer of molybdenum disulfide.[16–18]

For molybdenum disulfide, it is common to utilize the periodic ribbon model having a width of 4 rows of metal atoms with an idealized 'back' edge and two fixed 'rear' rows of metal and sulfur atoms (after this, the conventional model, Figure 1). Cells with four metal atoms along the edge are used most frequently. The edges are always metallic in the models having a periodicity of 4 or 2 metal atoms along the edge. However, there are assumptions that the edges are non-metallic, which is reproduced in models with a period ×3.[19] This discrepancy is a potential source of error. The width of a ribbon of four rows of Mo atoms is considered sufficient to exclude the interaction of the ribbon edges. A number of fundamental computational studies have been carried out on this model,[20,21] including those over the past few years.[7,22]

Bulk MoS_2 is diamagnetic. Only a limited propagation of the spin density from point substitutional defects in molybdenum disulfide[23] is observed. Similarly, the edge states are strongly localized.[24] Therefore, plotting the spin density penetration from the magnetic edge is a convenient tool for monitoring the perturbation of the electronic structure of the unperturbed diamagnetic molybdenum disulfide layer. Counting electrons on the edge molybdenum atom gives a fractional number of 1/3. In some calculation setups, this leads to artifacts.[19] In particular, electron density transfer between edge atoms or even between edges is possible as long as this allows to avoid fractional population of edge states.

The first aim of this work was to verify the scalability of the conventional ribbon model of the molybdenum disulfide edge and, if the scalability is imperfect, to find the optimal cell size. In particular, it is necessary to eliminate the inconsistency between the commonly used ×4 supercells and proposals to use the ×3 supercell for electron count reasons. The second aim was to evaluate the error introduced by the interaction of the edges and

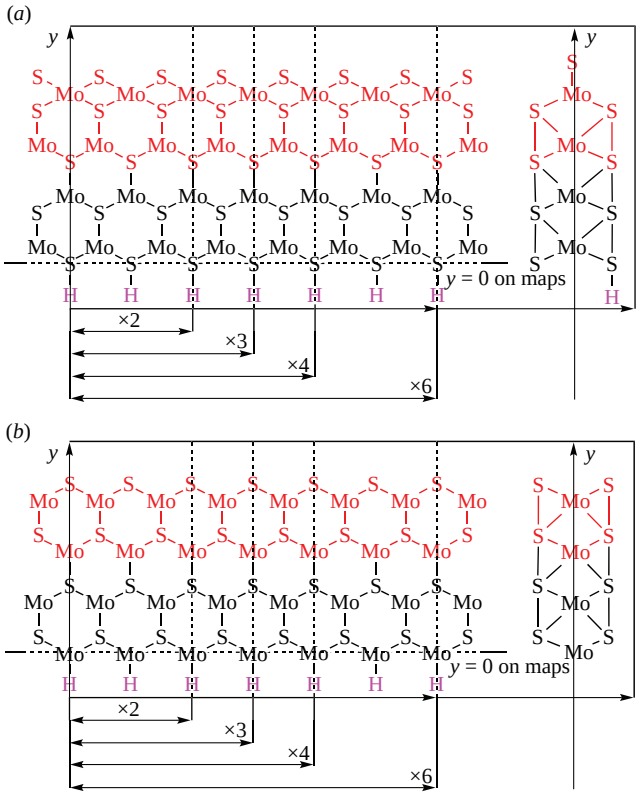

Figure 1 Supercell models used to calculate (*a*) the M edge and (*b*) the S edge. Mo and S atoms, differing in color in the upper and lower halves of the cells, are in relaxed and fixed positions, respectively. Additional hydrogen atoms are used to modify the 'back' edge.

to try to change the 'back' edge (namely, the opposite to the simulated one) in order to reduce its impact on the overall model. The third aim was to assess the importance of spin polarization for calculating the electronic structure of molybdenum disulfide. For this purpose, we calculated the specific energies of model supercells and constructed maps of the electron and spin density in the crystallite plane. We performed calculations without spin polarization with one *k*-point in the gamma position, similar calculations with spin polarization and calculations with spin polarization and a proportional number of *k*-points. We constructed a reference electron density for analysis of electron density distribution, averaging the density of ×2 and ×3 supercells between themselves and by ×1 shifts along the ribbon.

A computationally simple calculation with a gamma point without spin polarization is also the least accurate. There are significant differences in the specific energy of cells of different sizes for all models (Figure 2). In all cases, the specific energy of the ×2 cell is much higher than that of cells with other periods.

The electron density in the conventional ×2 model is reduced on all metal atoms except for the modeled M edge atoms and is increased compared to the reference density in the ×3 model (Figure S1). In the ×4 and ×6 models, the electron density on metal atoms in rows 2 and 3 is reduced, whereas a more likely polarization is observed at the 'back' edge (row 4). The electron density polarization pattern at the M edge is similar for the ×3–×6 pair, while the ×2 and ×4 models have their own patterns that differ from both ×3–×6 and each other. Polarization patterns at the 'back' edge are different for all models, but the ×4/×6 pairs are the closest to each other. The ×4 model has the lowest specific energy.

Presumably, the reason for such different distributions outside the boundaries of the simulated edge is a significant difference between the states of molybdenum and sulfur atoms at the 'back' edge from that characteristic of molybdenum. The difference is due to the high oxidation state of the molybdenum atoms at the 100% sulfided S edge and the low oxidation level where the 0% sulfided M edge has a low coordination number. This supercell model can be adjusted by modifying the 'back' edge with hydrogen. After such modification, the spread in edge energy between the cells increased (see Figure 2), while the difference in the electron density distribution remained essentially unchanged (Figure S2). This result means that such modification did not improve the quality of the model without spin polarization with gamma point.

The situation is different for the S edge. On the electron density difference map for the conventional model (Figure S3), reconstruction with the ×2 period occurs on the simulated S edge in the ×2 and ×4 cells; the reconstruction with the ×2 period in the ×6 cell and the reconstruction with the ×1 period in the ×3 cell are notably different. The electron density distribution at the 'back' edge is different for all cases. There is no scaling in either a ×2–×4–×6 row or a ×3–×6 row. The modification of the 'back' M edge with hydrogen (Figure S4) worsened the situation: the energy spread between the models increased, and reconstruction with the ×6 period appeared at the S edge in the ×6 cell.

Thus, the calculation in the diamagnetic gamma point approximation demonstrates unsatisfactory scaling of the M and S edges. This result may be due to an altered state of the edges caused by a change in the direction and degree of ribbon polarization. In this case, modifying the 'back' edge with hydrogen does not change the situation.

The first upgrade to the cheapest calculation is using the gamma point with spin polarization. The obtained specific energy data are presented in Figure 3. In the conventional model for both the M edge and S edge, the ×2 cell appears to be significantly higher in energy than the others. In the case of the M edge, the ×4 cell has the lowest energy, which contradicts the original expectations based on electron counting. For the S edge, the ×2, ×3 and ×4 models demonstrate, at first glance, a reasonably consistent specific energy value.

As seen on the electron density difference map for the conventional M edge model (Figure S5), the middle of the crystallite is electron-deficient for the ×2 cell and is enriched for the rest of the cells. A pronounced redistribution of the electron density with a period consistent with the model period is observed at the M edge in the cases of ×3, ×4 and ×6 cells. For ×4 and ×6 models, strong metal polarization at the 'back' S edge is in place. Surprisingly, the found energy of the ×6 cell was higher than that of ×3 and ×4 cells. This result is probably due to a different spin density distribution in the model (Figure S6).

For electron counting reasons, the energies of ×3 and ×6 cells should be lower than those of ×2 and ×4 cells, which contradicts the pattern observed for the conventional M edge model. However, for the model with the hydrogen-modified 'back' S edge, ×6 and ×3 cells are dramatically (by ~3 eV!) less in energy than ×2 and ×4 cells. This result is in complete agreement with the electron count. This model also has a rather complex pattern of electron density differences at the M edge, consistent with the cell period (Figure S7). The slightly higher energy of the ×6 cell compared to the ×3 cell can be explained by the complete absence of magnetism at the 'back' S edge in other models (Figure S8). Note that extraneous magnetism not associated with the modeled edge is the source of error.

Significantly different reconstructions in different supercells are observed on the map of the difference between the electron density and the reference density (Figure S9) for the conventional S edge model. The simulated edge in the ×6 model combines reconstruction elements for ×3 (electron-deficient S edge) and ×4 (reconstruction with the period of ×2) models, although there are no other similar elements on these maps. This combination is especially noticeable on the spin polarization map (Figure S10). The map clearly shows significant spin density in the middle of

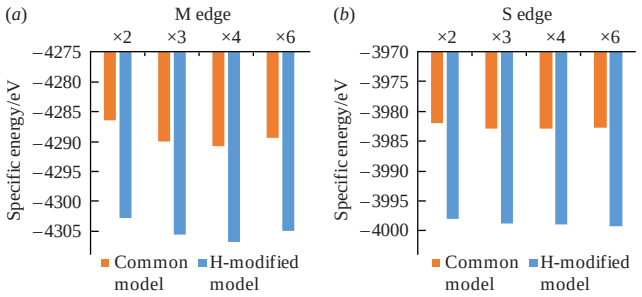

Figure 2 Specific energy (eV) of the model supercells per one crystal cell period, calculated for (*a*) the M edge and (*b*) the S edge without spin polarization with one *k*-point in the gamma position. The arrangement of atoms is shown in Figure 1.

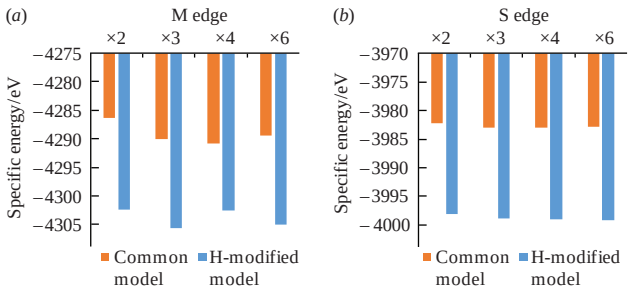

Figure 3 Specific energy (eV) of the model supercells per one crystal cell period, calculated for (*a*) the M edge and (*b*) the S edge with spin polarization and one *k*-point in the gamma position. The arrangement of atoms is shown in Figure 1.

the ribbon for the ×6 model, indicating edge interaction. Modification of the 'back' M edge with hydrogen led to an almost perfect scaling in energy of the ×2 and ×4 cells and the ×6 cell, which lies much lower in energy. However, the spin density map still shows significant spin density in the middle of the ribbon for the ×6 model, while the spin density in the middle of the ribbon is minimal in other models.

Calculations with the gamma point performed with spin polarization indicate a large difference between the specific energies of the edges in models with different supercell sizes. The dependence of the specific energy of a cell on its size with allowance for spin polarization significantly differed from that without spin polarization. Consequently, spin polarization can dramatically affect the calculated energy of the model and should be taken into account when calculating catalytic systems based on molybdenum disulfide. In addition, the ribbon model of molybdenum disulfide with a width of four rows of metal atoms may not be wide enough to isolate the edges, the interaction of which can be observed from the contact of the spin density associated with these edges (Figures S10 and S12).

Increasing the cell size in real space increases the density of the integration grid in the phase space proportionally. For correct comparison of cells of different sizes, the product of the number of *k*-points along the coordinate axis by the cell size along the axis should be the same (see Online Supplementary Materials). Moreover, since each *k*-point represents a separate electron wave, given their number, the effective number of electrons at the edge may be an integer, even if counting electrons directly gives a fractional number. In the last series of calculations with spin polarization in the same supercells, *k*-points were used, the number of which in the direction along the edge was inversely proportional to the cell size: 6, 4, 3 and 2 for the ×2, ×3, ×4 and ×6 cells, respectively. The product of the number of periods and the number of *k*-points remained unchanged. The integration grid in real and phase space had the same density for all investigated supercells. The conventional models of both the M edge and S edge had pairs of structures with similar energies but noticeable differences in the electronic structure. In particular, the energies of the ×2 and ×6 models for the M edge are close in magnitude; however, there are both significant deviations in the electron density map (Figure S13) and slight differences in the spin polarization pattern (Figure S14). These data mean that in this case, energy scalability by itself is not a sign of model scalability.

For the common M edge model, the minimum energy is found in the ×4 model, in which a characteristic reconstruction of the M edge with splitting molybdenum atoms into three types is observed. Since this reconstruction has the ×4 period, it cannot form in other supercells under study. Modifying the 'back' S edge with hydrogen does not fundamentally change the situation; the ×4 cell still has minimum energy. However, in contrast to the model with the unmodified 'back' S edge, a significant spin density is found on one of four atoms at the M edge in the ×4 cell and only on it in the case of the complete absence of spin polarization in other supercells (Figure S16). Regretfully, this casts doubt on the model with the hydrogen-modified 'back' edge since catalysts based on MoS_2 exhibit notable paramagnetism. In this case, no low-energy model with a period divisible by three was found. Apparently, the use of the number of *k*-points, which is a multiple of 3m, for the ×2 and ×4 models made it possible to create an effectively 'fractional' number of electrons at the edge, since the calculated structure was an averaging of three waves corresponding to different *k*-points.

For the S edge in the conventional model in ×2–×4 and ×3–×6 pairs (Figure S17), the electron density pattern is approximately repeated, and the energies of the models differ slightly (Figure 4). The edge state in the ×6 model is approximately average between

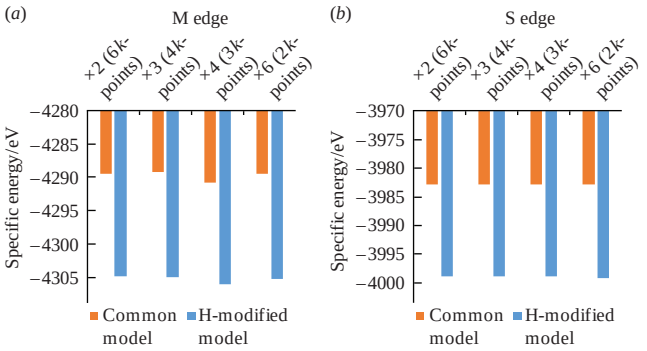

Figure 4 Specific energy (eV) of the model supercells per one crystal cell period, calculated for (*a*) the M edge and (*b*) the S edge with spin polarization and a proportional number of *k*-points. The arrangement of atoms is shown in Figure 1.

those in the ×3 and ×4 models but does not repeat any of them. The difference in spin distribution between ×2 and ×4 cells does not lead to an essential difference in energy. 'Back' edge modification with hydrogen results in the transition of the ×6 model into a state with model edge reconstruction with the ×6 period along the edge, which is accompanied by strong electric polarization of the 'back' edge (Figure S17). Moreover, only in this model, the spin density appears to be practically zero in the entire model (Figure S18). When using a proportional number of *k*-points, the ideal scalability of the MoS_2 catalyst ribbon model is not guaranteed. Besides, the modification of the 'back' edge with hydrogen can significantly reduce the perturbation of the electronic structure generated by this edge.

In conclusion, we found models that are close in specific energy but significantly different in electronic structure. Further, both the absolute and relative ordering of the specific energy of model supercells of different sizes turned out to be sensitive to spin polarization, modification of the structure of the 'back' edge and the use of a proportional number of *k*-points. In particular, calculations using a gamma point at the M edge with hydrogen-modified 'back' edge showed that a fractional specific number of electrons at the edge could cause a difference in specific energies, amounted to a few electronvolts, between models of the calculated edge with different supercell sizes. Therefore, special attention should be paid to electron counting in calculations with the gamma point in the MoS_2 ribbon model. We also propose to ensure that there is no edge interaction, particularly the electron density perturbation generated by the modeled and 'back' edges, which should be isolated from each other. The use of a ribbon with four rows of molybdenum atoms is usually, but not always, enough to prevent contact between the zones of influence of the ribbon edges, preventing them from interacting.

The Scientific Schools Development Program by the N. D. Zelinsky Institute of Organic Chemistry is gratefully acknowledged. For some calculations, the supercomputer resource of the Joint Supercomputer Center of the Russian Academy of Sciences was used.

Online Supplementary Materials

Supplementary data associated with this article can be found in the online version at doi: 10.1016/j.mencom.2021.07.032.

References

1 A. Tanimu and K. Alhooshani, *Energy Fuels*, 2019, **33**, 2810.
2 H. T. Luk, C. Mondelli, D. C. Ferré, J. A. Stewart and J. Pérez-Ramírez, *Chem. Soc. Rev.*, 2017, **46**, 1358.
3 W. Luo, H. Shi, E. Schachtl, O. Y. Gutiérrez and J. A. Lercher, *Angew. Chem., Int. Ed.*, 2018, **57**, 14555.

4 Z. Li, D. Zhang, J. Ma, D. Wang and C. Xie, *Mater. Lett.*, 2018, **213**, 350.
5 W. Han, S. Wang, X. Li, B. Ma, M. Du, L. Zhou, Y. Yang, Y. Zhang and H. Ge, *RSC Adv.*, 2020, **10**, 8055.
6 R. Arancon, M. Saab, A. Morvan, A. Bonduelle-Skrzypczak, A.-L. Taleb, A.-S. Gay, C. Legens, O. Ersen, K. Searles, V. Mougel, A. Fedorov, C. Copéret and P. Raybaud, *J. Phys. Chem. C*, 2019, **123**, 24659.
7 P. Zheng, A. Duan, K. Chi, L. Zhao, C. Zhang, C. Xu, Z. Zhao, W. Song, X. Wang and J. Fan, *Chem. Eng. Sci*., 2017, **164**, 292.
8 A. S. Rosen, J. M. Notestein and R. Q. Snurr, *J. Phys. Chem. C*, 2018, **122**, 15318.
9 K. Zhang, W. Wang, B. Wang, X. Ma and Z. Li, *Appl. Surf. Sci*., 2019, **463**, 635.
10 Y.-Y. Chen, M. Dong, Z. Qin, X.-D. Wen, W. Fan and J. Wang, *J. Mol. Catal. A: Chem*., 2011, **338**, 44.
11 Y. Sayed-Ahmad-Baraza and C. P. Ewels, *Chem. – Eur. J.*, 2020, **26**, 6686.
12 M. V. Bollinger, K. W. Jacobsen and J. K. Nørskov, *Phys. Rev. B*, 2003, **67**, 085410.
13 S. Manzeli, D. Ovchinnikov, D. Pasquier, O. V. Yazyev and A. Kis, *Nat. Rev. Mater*., 2017, **2**, 17033.
14 U. Krishnan, M. Kaur, K. Singh, M. Kumar and A. Kumar, *Superlattices Microstruct*., 2019, **128**, 274.
15 Q. Fang, X. Zhao, Y. Huang, K. Xu, T. Min and F. Ma, *J. Mater. Chem. C*, 2019, **7**, 3607.
16 D. Wu, X. Li, L. Luan, X. Wu, W. Li, M. N. Yogeesh, R. Ghosh, Z. Chu, D. Akinwande, Q. Niu and K. Lai, *Proc. Natl. Acad. Sci. USA*, 2016, **113**, 8583.
17 S. Krishnamurthi and G. Brocks, *Phys. Rev. B*, 2020, **102**, 161106.
18 K.-I. Lin, Y.-H. Ho, S.-B. Liu, J.-J. Ciou, B.-T. Huang, C. Chen, H.-C. Chang, C.-L. Tu and C.-H. Chen, *Nano Lett.*, 2018, **18**, 793.
19 M. C. Lucking, J. Bang, H. Terrones, Y.-Y. Sun and S. Zhang, *Chem. Mater*., 2015, **27**, 3326.
20 M. Sun, A. E. Nelson and J. Adjaye, *J. Catal.*, 2004, **226**, 41.
21 E. Krebs, A. Daudin and P. Raybaud, *Oil Gas Sci. Technol*., 2009, **64**, 707.
22 F. Caron, M. Rivallan, S. Humbert, A. Daudin, S. Bordiga and P. Raybaud, *J. Catal.*, 2018, **361**, 62.
23 R. Mishra, W. Zhou, S. J. Pennycook, S. T. Pantelides and J.-C. Idrobo, *Phys. Rev. B*, 2013, **88**, 144409.
24 A. Parija, Y.-H. Choi, Z. Liu, J. L. Andrews, L. R. De Jesus, S. C. Fakra, M. Al-Hashimi, J. D. Batteas, D. Prendergast and S. Banerjee, *ACS Cent. Sci*., 2018, **4**, 493.

Received: 22nd January 2021; Com. 21/6427